CHEMISTRY OF MATERIALS

pubs.acs.org/cm

Article

Understanding the Activation of ZSM-5 by Phosphorus: Localizing Phosphate Groups in the Pores of Phosphate-Stabilized ZSM-5

Jaap N. Louwen, Lambert van Eijck, Charlotte Vogt, and Eelco T.C. Vogt*

Cite This: *Chem. Mater.* 2020, 32, 9390−9403

Read Online

ACCESS | Metrics & More | Article Recommendations | Supporting Information

ABSTRACT: Fluid catalytic cracking (FCC) produces (the feedstock for) a major part of the world's fuels, as well as chemical building blocks for, for example, polymers, pharmaceuticals, and specialty materials. ZSM-5 is the active ingredient in propylene-selective FCC catalyst systems and is stabilized or activated with phosphorus compounds. Despite this process being one of the largest-scale industrially applied catalytic processes, there is still considerable debate on the mechanism of activation, as well as on the interaction between phosphate and zeolite aluminum species. In this work, we use synchrotron-based powder XRD, neutron diffraction, and subsequent pair distribution function analysis to unequivocally corroborate the activation mechanism of phosphorus-based promotion in FCC catalysis and localize the phosphate groups inside the pore system of P-activated ZSM-5. We find local disorder in the zeolite T−O coordination, which could not be observed with traditional XRD analyses. Furthermore, we support these experimental findings with full periodic quantum-mechanical modeling (QMM) of the highly relevant, but often overlooked, combination of dealumination by hydrolysis (steaming) and phosphatation of the zeolite framework. We thereby show that phosphate can react with partially dislodged aluminum species that remain stable and are still tethered to their original framework position. Finally, by assessing all available literature postulations by the same periodic QMM and comparing them energetically with our obtained results, we can conclude that by accounting for the highly relevant inclusion of steaming prior to phosphatation, the two models resulting from this work rank among the three most relevant remaining models. This combined experimental and theoretical work fundamentally explains the activation and promotion mechanism of one of the world's most applied chemical processes—propylene-selective FCC.

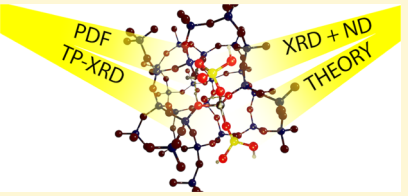

1. INTRODUCTION

There is currently no scalable alternative for the production of fuels and materials from crude oil. While working on fossil-fuel alternatives, it is equally important for scientists to fundamentally understand and thereby attempt to minimize the environmental impact of current crude oil-based processes such as fluid catalytic cracking (FCC), the major conversion technique used to produce gasoline from oil fractions. The FCC process is also increasingly used to produce propylene, a key intermediate for the production of polyolefins, and has become the second largest source of propylene (steam cracking of naphtha is the largest source). The propylene-selective FCC process uses approximately 90,000 tons of catalysts per year[1] to produce approximately 30% of an estimated global market of 100 million metric tons of propylene.[2−4] The remainder of propylene is conventionally produced by the aforementioned steam cracking and on-purpose processes such as propane dehydrogenation, but considerable additional processing capacity is needed to supply demand that cannot be met with these processes.[2−4] Even incremental improvements to chemical processes of such immense scale have a significant and direct impact on harmful environmental emissions.

The active component in the propylene-selective FCC catalyst or catalyst additive is the zeolite ZSM-5, which is typically treated with a phosphorus component such as phosphoric acid to promote activity. The empirically found optimal activation procedure for zeolite depends on several factors, including the silicon-to-aluminum ratio in zeolite,[5−18] the specific P component used,[19−24] the activation conditions (such as the ratio of P to Al or impregnation conditions such as concentration and temperature), and especially, the final heat treatment (steaming and/or calcination).[5,11−13,18,25,26] It is known that the addition of phosphate to the zeolite leads to a reduction of acid-site quantity and acid-site strength,[20,22,26−29] reduction of the pore volume,[6,16,21,30] and formation of diffusion barriers.[6] However, because of the large variation in materials and (preparation) procedures,[31] it must be noted that it is very difficult to compare literature results. Hence, arguably, a large degree of variation exists in theories explaining the activation mechanism (see also Figure 1a−h which schematically shows the available explanations).

Nevertheless, it is clear that P-activated ZSM-5 outperforms steamed H-ZSM-5, as demonstrated by the catalytic test data in the Supporting Information.[32] This either implies that more

Received: August 21, 2020
Revised: October 5, 2020
Published: October 19, 2020

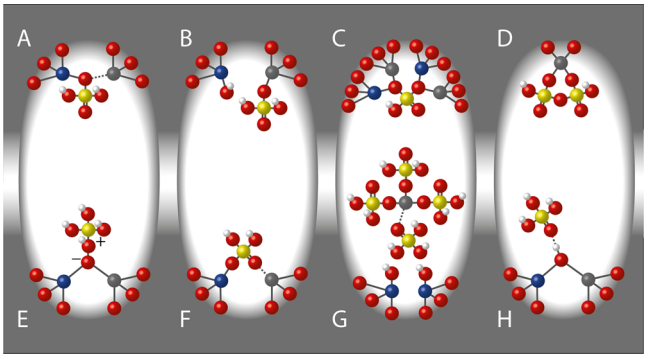

Figure 1. Current models in the literature explaining the activation mechanism of phosphate ZSM-5. Red spheres are oxygen atoms, blue: silicon, gray: aluminum, yellow: phosphorus, and white: hydrogen. (a) Kaeding and Butter,[19] (b) Zhuang et al.,[7] (c) Xue et al.,[13] (d) van der Bij et al.,[22] (e) Blasco et al.,[5] (f) Lercher et al.,[27] (g) Caro et al.,[6] and (h) Abubakar et al.[10] The image is based on ref 33.

aluminum atoms stay in their tetrahedral framework sites leading to Brønsted acidity, as Caeiro et al. suggest,[25] or new acid species are formed because of the direct interaction of phosphate with the zeolite framework, as proposed by, for example, Xue et al.[17] Various other authors propose models for the interaction of phosphate with the zeolite framework. Except for the model by van der Bij and Weckhuysen,[22] none of the models take into account the combination of prior dealumination by steam and phosphatation, while this is a highly relevant inclusion as most experimental procedures apply a calcination step prior to phosphatation. Kaeding and Butter, starting from trimethylphosphite as the reagent, propose a site where phosphate is bound through an Si−O−P bond and coordinated to Al via one of the P−OH groups (Figure 1a).[19] Zhuang et al. propose a reaction between phosphate and aluminum, which leads to the formation of a $(SiO)_x$−Al−O−P bond and the breakage of the original Si−OH−Al bond (Figure 1b).[7] The model by Xue et al.[13] assumes the condensation reaction of two P−OH groups of a single phosphate species with two separate Si−OH−Al Brønsted acid groups as a first step (Figure 1c). Van der Bij et al.[22] propose a reaction of two phosphate species to partially dislodged alumina obtained by the action of steam on the framework (Figure 1d). Blasco et al. propose protonation of the phosphate group by the Brønsted acid site (Figure 1e).[5] Lercher and Rumplmayr[27] suggest the formation of Si−O−P−O−Al bonds by replacing the original Brønsted acid site hydroxyl with a bridging $H_2PO_4^-$ (Figure 1f). Caro et al. propose the formation of phosphated, completely dislodged extra framework Al and silanol nests (Figure 1g)[6] and Abubakar et al. propose an interaction of the P=O oxygen with the Brønsted acid site with additional hydrogen bridges from the P−OH groups to the framework oxygens (Figure 1h).[10] Van der Bij and Weckhuysen suggest that the first step is partial dislodging of the Al from the framework through hydrolysis of Si−O(H)−Al bonds by steam. The partially dislodged Al species can then react with multiple phosphate groups by condensation of P−OH groups with Al−OH groups. This latter explanation is fundamentally different from the other models, which all assume direct action of the phosphate (precursor) with the Brønsted Si−O(H)−Al species.

It should be clear that there is considerable dispute as to the exact nature of changes the local environment around the aluminum in the framework undergoes by reaction with phosphate. In this work, we will attempt to provide clarity on this issue by, to the best of our knowledge, for the first time, refining the long-range crystal structure of activated ZSM-5, as well as by investigating the short-range order, and we will examine the relative energetics of the various proposed structures with quantum-mechanical modeling, all the while including dealumination in the mechanism as done by van der Bij and Weckhuysen. In a previous study using atom probe tomography (APT),[32] our group has demonstrated that Al atoms remain in the vicinity of their framework position, with phosphate groups in direct proximity with an Al/P ratio close to 1. Furthermore, with ^{1}H, ^{29}Si, ^{27}Al, and ^{31}P magic-angle spinning NMR spectroscopy, we demonstrated that the majority of the Al was in a distorted electronic environment, partially caused by direct interaction with P, and apparently, no longer involved in Si−O(H)−Al Brønsted acid sites. ^{1}H MAS NMR spectra also indicated the possibility of formation of new acid sites from P−OH groups.[32]

Here, we will use synchrotron XRD and neutron diffraction (ND) structure refinements to localize phosphate groups inside the pores of P-activated ZSM-5, demonstrating that P atoms migrate into the pores and react with Al atoms in the vicinity of their original positions. Furthermore, we will show that short-range order derived from atom-pair distribution functions is different from the long-range order found in the XRD and ND refinements, showing that previous conclusions based on the long-range order deviate from reality. Furthermore, the structural strain and framework damage will be examined by assessing the temperature dependence of the orthorhombic−monoclinic phase transition in the ZSM-5 framework. We will use quantum-mechanical modeling (QMM) to conclude that the inclusion of steaming prior to phosphatation is important to provide relevant models. We show that the phosphate group or groups can provide additional acid sites, for which we calculate the acidity to be

Table 1. Overview of the Samples and Methods Applied in This Study[a]

	Si/Al (EDX)	P/Al	XRD/ND	PDF	TP-XRD
parent ZSM-5	9.9	0	XRD: 85 K, RT; ND: RT	XRD: 85 K; ND: RT	X
0.8 P-treated ZSM-5	9.8	0.8	XRD: 85 K, RT; ND: RT	XRD: 85 K; ND: RT	X
5.0 P-treated ZSM-5	39.3	5.0		XRD: 85 K	X
steamed parent	n.d.	0			X
ZMS-5 SAR 41.5	n.d.	0			X
ZSM-5 SAR 120	n.d.	0			X

[a]More details can be found in ref 32.

https://dx.doi.org/10.1021/acs.chemmater.0c03411
Chem. Mater. 2020, 32, 9390−9403

equivalent to the original Brønsted sites. This implies the existence of a stabilization mechanism keeping the aluminum atoms close to their original framework sites and introducing multiple additional acid sites inside the pore system. The model also explains the diffusion barriers observed by, for example, Caro et al.,[6] as the phosphate groups inside the pores hinder diffusion. To conclude, our proposed model provides a comprehensive explanation for the activation mechanism in one of the most important industrial catalytic processes—propylene-selective FCC.

2. EXPERIMENTAL DETAILS

2.1. Samples. The samples used in this study have been described before.[32] We used commercial H-ZSM-5 to prepare phosphate-stabilized ZSM-5. As the experimental focus in this paper is on the structure of activated ZSM-5, the study of the actual additive, with the activated ZSM-5 embedded in a matrix, is beyond the scope of this paper. The silica/alumina molar ratio of the material was 25 (Si/Al ratio 12.5) based on supplier information. The material was calcined at 550 °C, and subsequently, suspended in a solution of dilute phosphoric acid to create samples with a final P/Al ratio of 0.8 and 5.0, respectively. The samples were filtered, washed, and dried at 120 °C, and finally calcined at 550 °C. For comparison, we also studied the parent material, a steamed version of the parent material, a P-free sample of ZSM-5 with a Si/Al ratio of 41.5, and a P-free sample of ZSM-5 with a Si/Al ratio of 120. More details on the samples, including activity data, can be found in Danisi et al.[32] Table 1 shows an overview of the samples and the methods applied in this work.

2.2. X-ray Diffraction. Synchrotron XRD and scattering patterns were recorded at the high-resolution diffraction beamline ID-22 at ESRF in Grenoble, France. Total scattering analysis was performed at an X-ray photon energy of 65 KeV (wavelength 0.19071 Å) using a flat panel PerkinElmer XRD 1611CP3 Detector with 4196 by 4196 pixels (detector area: 41 × 41 cm^2, pixel size: 100 × 100 μm^2). Data were collected for 5 s per frame and 200 frames were averaged and integrated to obtain the final 1D dataset. Averaging of the 2D data and integration of the diffraction rings were done with the local (ESRF) program pyFAI.[34,35] The 2D detector was placed at 55 cm from the sample capillary to increase the resolution. The beam was focused on the sample or detector using a transfocator. For the collection of the total scattering data, the transfocator was focused on the sample, leading to a higher intensity at the cost of Q-resolution. Prior to the total scattering collection at each temperature, the transfocator was focused on the detector to allow recording of five frames at higher Q-resolution, for analysis of the structural changes (monoclinic to orthorhombic transition, dehydration effects). Data were collected at 85, 100, 145, 155, 165, 175, 185, 195, 309, 400, 500 K, and finally at 150 K for the low-silicon-to-aluminum ratio (SAR) samples. Temperature was controlled with a cryostream. Ramps between temperatures were done at 6 K per minute, while single images were collected for 5 s, every 8 s. Total scattering backgrounds were collected with the transfocator out (focusing on the sample) with an empty capillary. The resulting averaged and integrated datasets were analyzed with xPDFsuite (based on PDFgetX3[36]).

The powder XRD patterns of these samples were recorded with a fixed wavelength of 0.399961(2) Å (X-ray photon energy: 31 KeV) on the ID-22 diffractometer at ESRF (Rotary Precision Instruments, UK). The diffractometer uses a nine-channel detector bank, with the channels two degrees apart, in which each channel is preceded by a Si-111 analyzer crystal. The diffraction data were collected from spinning capillaries at room temperature, and subsequently, after waiting for some time to achieve phase "re-equilibration", at low temperatures (85 K). The temperature was controlled with a cryostream. The background was recorded with an empty capillary.

2.3. Neutron Diffraction. ND patterns were recorded on the PEARL diffractometer at Delft University[37] at room temperature using three different wavelengths (selecting three different reflections in the germanium monochromator) to cover both high and low ranges of Q-values (the first peaks in the diffraction pattern of ZSM-5 appear at around Q = 0.5 $Å^{-1}$, and are not visible in the pattern recorded at 1.098 Å), see Table 2. Data were collected over a 2-theta range of 10.58−158.98 degrees with a pixel angular width of approximately 0.105 degrees. For the analysis of the total scattering functions from constant-wavelength ND data, a new version of the program PDFgetX3,[36] called PDFgetN3, was developed in cooperation with the group of Billinge.[38]

Table 2. Three different Wavelengths Used in ND Experiments and the Resulting Q-Ranges.

reflection	wavelength (Å)	Q_{min} ($Å^{-1}$)	Q_{max} ($Å^{-1}$)
755	1.098788	1.054	11.245
533	1.667181	0.695	7.411
133	2.507877	0.462	4.927

The data were collected for approximately 24 h. Scattering intensities from the vanadium sample holder and the instrumental background were measured separately. The resulting datasets were analyzed with PDFgetN3.[38]

All crystallographic analyses (except for PDF analysis) were done with the program TOPAS, version 6, as marketed by Bruker-AXS.[39] We applied X-ray scattering factors as published in the literature for the X-ray synchrotron data[40] and the neutron coherent scattering lengths.[41] The exact parameters used can be found in the Supporting Information. It should be noted that the data sets applied with TOPAS do not provide values for the anomalous scattering factors f′ and f″ at a wavelength of 0.4 Å, so these values were set to zero, which is an acceptable approximation for the elements involved (O, Al, Si, and P).

2.4. Computational Details. Quantum-mechanical calculations were performed with the CP2K−Quickstep module (version 4.1)[42−46] on full periodic models of the MFI-unit cell without symmetry constraints (space group P1), using the PBE density functional[47] and the MOLOPT-DZVP basis set[48] with Goedecker−Teter−Hutter (GTH) pseudopotentials.[49−51] We did not apply dispersion corrections as previous results show that these do not significantly influence the reaction profiles in this type of study.[52,53] The standard basis set and pseudopotentials, as distributed with the CP2K-program, were used. We deviated from the default program settings for the cutoff energy for the finest grid level, which was increased to 700 Rydberg units, as well as the target accuracy for SCF, which was increased to 10^{-7} charge units. We only calculated the gamma point; no integration over the Brillouin zone was performed. All atom coordinates were optimized in a fixed unit cell. The unit cell was kept constant at a volume derived from experiment, a = 20.12343 Å, b = 19.95413 Å, c = 13.42174 Å, and $\alpha = \beta = \gamma = 90°$, based on a room-temperature powder profile refinement of one of the samples. We compared this result with a fully unconstrained framework and atom-coordinate optimization of all-silica MFI. This led to a = 20.174 Å, b = 20.380 Å, c = 13.574 Å, $\alpha = \gamma = 90°$, and β = 90.4°, and a framework energy lower by 4.4 kcal/mol compared to the experimentally derived unit cell volume. We consider this difference sufficiently small given the presence of 288 atoms in the unit and will use the experimentally derived cell in our calculations for this study.

3. RESULTS AND DISCUSSION

3.1. Long-Range Order: X-ray Diffraction and Neutron Diffraction Analyses. To facilitate the localization of potential extra-framework content induced by the stabilization of ZSM-5 with phosphorus, we first need to accurately model the framework of the ZSM-5 parent material. We performed a structure refinement on a synchrotron XRD powder pattern of the parent ZSM-5 recorded at 85 K (see the Supporting Information paragraphs 1.1 and 2.1). This refinement led to the structure shown in Figure 2a and is a structure that—upon

https://dx.doi.org/10.1021/acs.chemmater.0c03411
Chem. Mater. 2020, 32, 9390−9403

visual inspection—seems more ordered than the Olson model.[54]

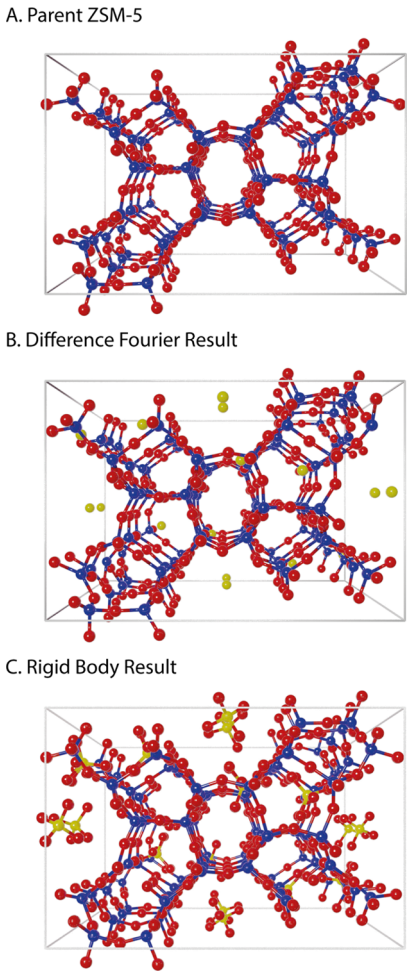

Figure 2. X-ray structure solutions at 85 K for the structure of (a) the parent material and the (b,c) 0.8 P-ZSM-5 sample. The middle solution for the P-ZSM-5 sample (b) was obtained by Fourier-map analysis. The bottom solution (c) was derived with the rigid-body technique, in which PO_4 tetrahedra were introduced as rigid bodies. The a-axis is the horizontal axis, the c-axis is the vertical axis, and the b-axis points away from the viewer.

3.1.1. XRD Structure Refinement of the 0.8 P/Al Sample: Difference Fourier Analysis. Subsequently, we performed structure refinements on the phosphated sample 0.8 P/Al based on synchrotron powder profiles recorded at 85 K and room temperature. We refined the structures with two independent refinement techniques, that is, conventional difference Fourier analysis and rigid body analysis. In the difference Fourier analysis, we used the structure refined for the parent (above) to create a difference Fourier map (i.e., in essence, we subtracted the electron density from the zeolite lattice to leave only that of the species in the pores). After doing a profile refinement on a partial model (starting from the structure for the parent material), difference electron density maps are computed based on the refined structure factors as well as on the structure factors obtained by distributing the observed intensities in proportion to the refined structure factors. Each time, a P atom is placed at the locus of the highest density difference that is not associated with a framework atom, giving the next partial model to be refined. For the scan recorded at 85 K, we find we can place three P atoms. At this point, the difference density map shows no significant unexplained density anymore. The same procedure applied to the scan recorded at RT gave four such P atoms. The results are given in Table 3. The profile fits are reported in Section 2 of the Supporting Information. With the difference Fourier refinement strategy, it was not possible to gather information about the location of the oxygen atoms of the phosphate groups. The occupation factors of the P atoms were refined to values in excess of unity using the scan recorded at 85 K, while the refined Debye–Waller factors are all at the maximum allowed value of 20 $Å^2$. We take the nominal location of the P atoms to signify the approximate position of the center of mass of the (presumably more or less randomly oriented) phosphate groups. The higher refined occupation for the scan recorded at 85 K compared to the scan recorded at RT apparently reflects a lower degree of mobility at that temperature.

We should note that, based on APT and chemical analyses reported in our previous work,[32] we would expect to find approximately seven or eight P atoms per unit cell.

3.1.2. XRD Structure Refinement of the 0.8 P/Al Sample: Direct Space—Rigid Body Analysis. In addition to the difference Fourier analysis, we also applied a direct space method, which was applied without using the information from the difference Fourier analysis. Using the simulated annealing procedure, as implemented in TOPAS, we attempted to place rigid PO_4 tetrahedra (P–O distance: 1.54 Å) into the pores of the structure refined for the parent material. For the scan recorded at 85 K as well as the scan recorded at RT, we can achieve a significant improvement in the fit between observed and computed scans when we place up to three PO_4 tetrahedra in this way, using position, orientation, and occupation factor for each tetrahedron as degrees of freedom. In all cases, introducing a fourth PO_4 tetrahedron gives no significant improvement, and the occupation factor of the fourth tetrahedron is refined close to zero. Removal of the constraint of tetrahedral symmetry on the PO_4 units leads to unphysical distortions of the PO_4 geometries upon further refinement. For comparison with the results obtained by the difference Fourier analysis approach, the results (only the coordinates of the central P atom) are shown in Table 3. We find a fair agreement between the positions of the central atom obtained from the 85 K and RT scans. The occupation numbers are clearly considerably smaller than those found in the difference Fourier analysis approach, which is understandable as, in that case, the single P atom had to account for the total difference electron density of the phosphate groups, and we now have four oxygen atoms with the same occupation factor. The refined Debye–Waller factors found when modeling with PO_4 tetrahedra rather than P atom factors are considerably smaller (all in the range of 3–14 $Å^2$), showing an improved modeling of the difference electron density by the tetrahedra. As before, we find smaller occupation factors for results obtained from the RT scan compared to those for results from the 85 K scan.

The positions of the central P atoms of the tetrahedra match well with the positions found for the P atoms in the difference Fourier analysis based on the 85 K scan, which renders the difference Fourier analysis results obtained from the RT scan, with its four P atom positions, not optimal.

3.1.3. Combination of XRD and ND Data. In order to improve the models refined at RT, we performed a

https://dx.doi.org/10.1021/acs.chemmater.0c03411
Chem. Mater. 2020, 32, 9390–9403

Table 3. Summary Table with All XRD Synchrotron Analysis Results

	space group	*a*	*b*	*c*	*α*	*β*	*γ*	unit cell volume	R_{exp} (%)	R_{wp} (%)	R_{Bragg} (%)
parent	*Pnma*	20.132	19.950	13.426	90.000	90.000	90.000	5392.624			
Fourier 85 K	*Pnma*	20.078	19.922	13.415	90.000	90.000	90.000	5365.935	2.4	6.6	2.3
rigid body 85 K	*Pnma*	20.071	19.916	13.410	90.000	90.000	90.000	5360.271	2.4	5.5	1.8
Fourier RT	*Pnma*	20.090	19.926	13.416	90.000	90.000	90.000	5370.341	2.5	6.0	1.3
rigid body RT	*Pnma*	20.086	19.923	13.412	90.000	90.000	90.000	5367.078	2.5	5.7	1.2
			x		*y*		*z*	occupancy		B_{iso}	
Fourier 85 K	P1		0.994		0.131		0.539	1.408[a]		20.000	
	P2		0.242		0.250		0.858	1.391[a]		20.000	
	P3		0.050		0.250		0.810	1.672[a]		20.000	
rigid body 85 K	P1		0.007		0.131		0.509	0.621		14.029	
	P2		0.259		0.250		0.849	0.563		14.567	
	P3		0.057		0.250		0.801	0.655		2.915	
Fourier RT	P1		0.007		0.022		0.446	0.359		20.000	
	P2		0.284		0.250		0.862	0.567		20.000	
	P3		0.085		0.250		0.803	0.652		20.000	
	P4		0.027		0.250		0.530	0.759		20.000	
rigid body RT	P1		0.012		0.110		0.567	0.300		12.340	
	P2		0.349		0.250		0.861	0.189		10.313	
	P3		0.092		0.250		0.815	0.235		7.814	

[a]We observe occupancy numbers larger than one at 85 K because we are trying to model the difference electron density of phosphate groups with phosphorus atoms, and we have to account for the electron density of the oxygen atoms (see the text below).

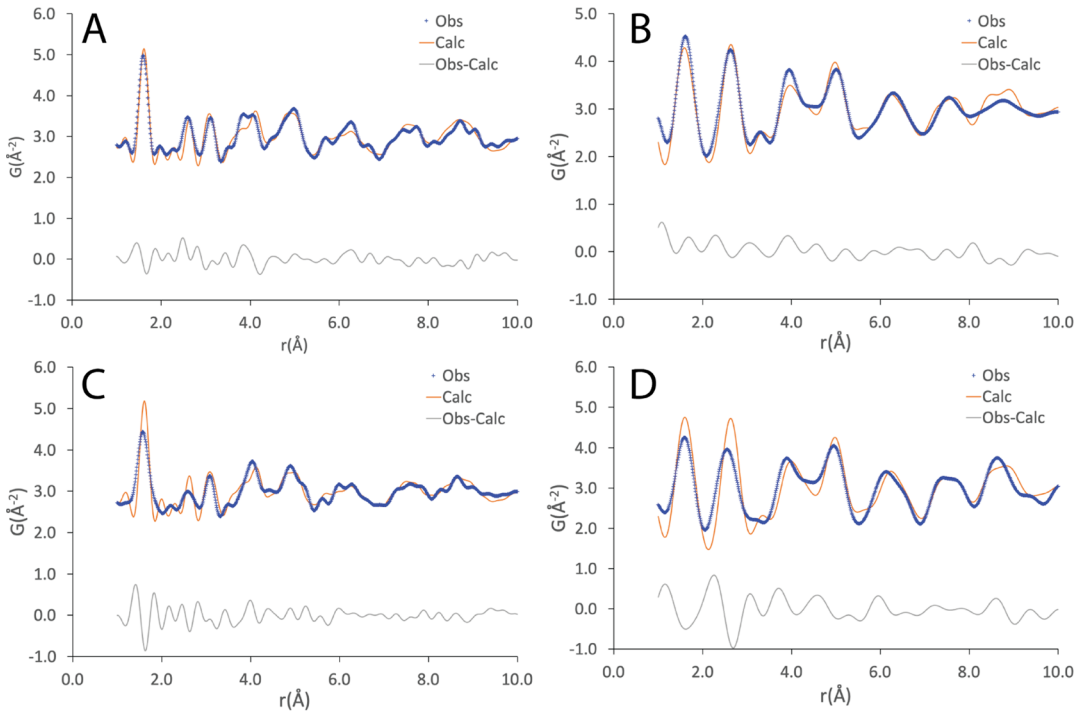

Figure 3. Atom pair distribution functions from total scattering analysis. (a) XRD (85 K) analysis and (b) neutron PDF (RT) analysis of the parent material and (c) XRD (85 K) analysis and (d) neutron PDF (RT) analysis of the 0.8 P/Al-material. The refinement was limited to profile parameters; the PDFs for the parent material were fitted to the structure found from synchrotron X-ray full profile refinement for the parent material at 85 K. The PDFs for the 0.8 P/Al sample were fitted to the rigid-body model refined at 85 K and RT, respectively. The neutron PDFs were derived from diffraction patterns recorded at a wavelength of 1.098 Å to gather data at the largest possible *Q*-values.

simultaneous refinement on the synchrotron XRD scan and the three ND scans recorded at different wavelengths. As we only have data for RT ND, we could not perform this analysis at 85 K. The detailed results for this refinement are reported in the Supporting Information, Section 2.6. In the Supporting Information, we also have provided additional results for the refinement based only on the three ND scans. Because of the lower signal to noise ratio and overlapping peaks, these results do not provide a better fit of the data. For both the difference Fourier analysis and the direct space results, the changes are minimal compared to the XRD solutions.

The (single P atom) results from difference Fourier analysis appear to be less consistent compared to those obtained by the direct space approach, possibly because the latter uses a more

https://dx.doi.org/10.1021/acs.chemmater.0c03411
Chem. Mater. 2020, 32, 9390−9403

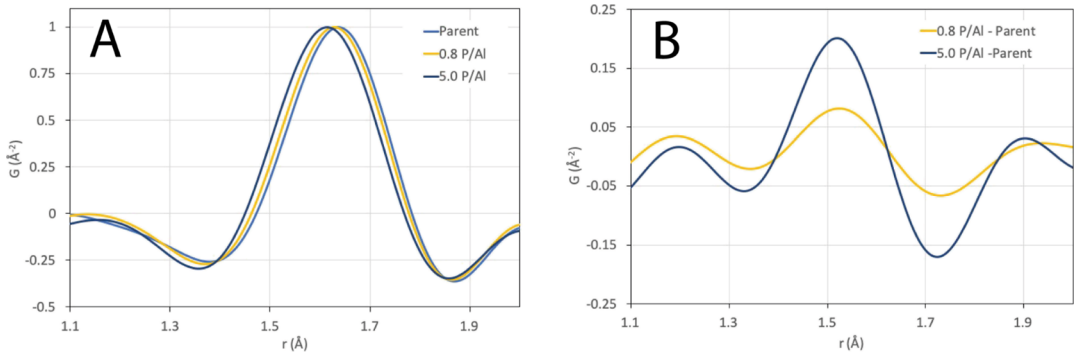

Figure 4. (a) Details of the T−O range in the PDFs for parent HZSM-5, 0.8 P/Al ZSM-5, and 5.0 P/Al ZSM-5. (b) Difference between 0.8 P/Al ZSM-5 and the parent and between 5.0 P/Al ZSM-5 and the parent. The difference peaks increase in height with increasing P content, and the peak at 1.54 Å is exactly the expected length for the P−O bond. As the PDFs are normalized to the height of the major peak, the *y*-axis is arbitrary.

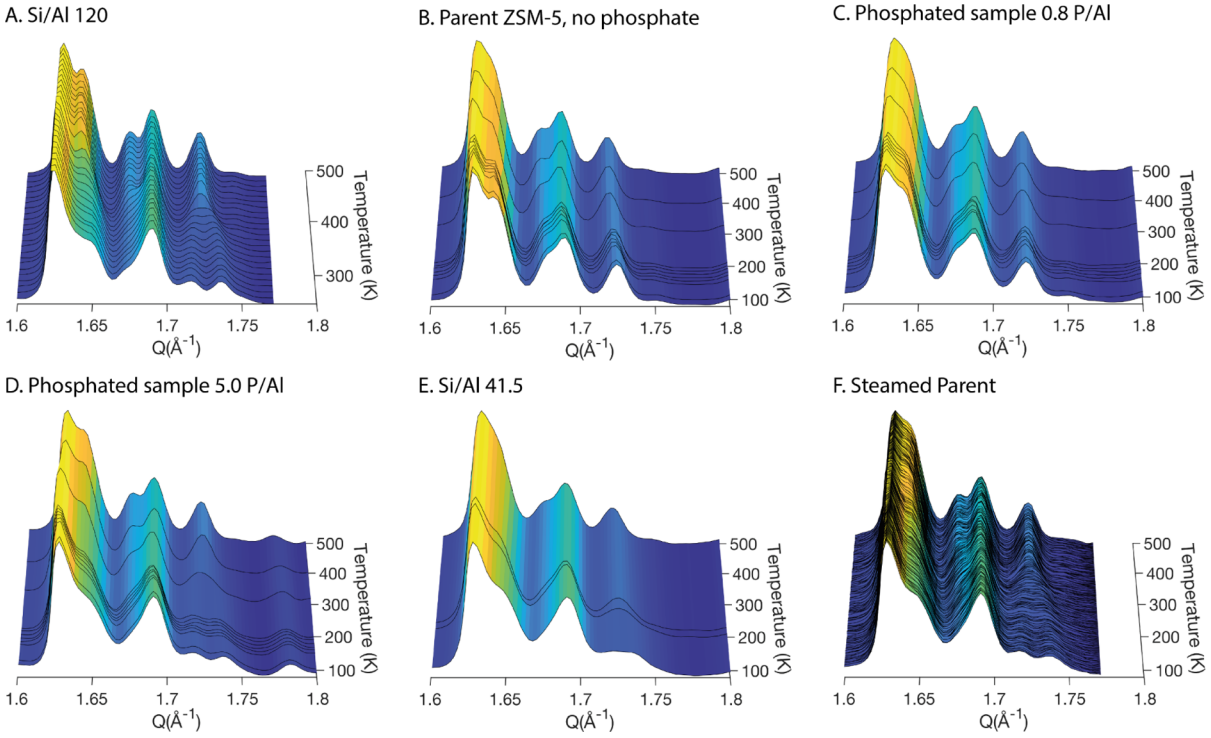

Figure 5. Monoclinic−orthorhombic transition of six ZSM-5 samples as a function of temperature. The *Z*-axis normalized on the highest peak in the range. (a) Si/Al ratio of 120, no phosphorus treatment. This sample most clearly shows the monoclinic−orthorhombic transition: At low temperatures, the splitting of the 133 peak (orthorhombic) into the −313/313 doublet (monoclinic) is evident in the Q = 1.72−1.74 $Å^{-1}$range. The transition temperature (defined as the temperature halfway of the trajectory) is about 105 °C. (b) Parent material (Si/Al ratio: 12.5), no P treatment. No monoclinicity is observed even at 85 K. (c) 0.8 P/Al ZSM-5 with an initial Si/Al ratio of 12.5. No monoclinicity is observed even at 85 K. (d) 5.0 Al/P ZSM-5 with an initial Si/Al ratio of 12.5. The splitting at low T is less well defined as in the Si/Al 120 sample, and the transition trajectory is much longer. The transition takes place close to room temperature. (e) Si/Al: 41.5. The transition is visible, but poorly defined. (f) Steamed parent material, no P treatment. The transition takes place close to room temperature.

realistic rendering of the difference electron density of a phosphate group. Nevertheless, the fact that the direct space method yields positions for the central P atom of the tetrahedra that correspond with the results of difference Fourier analysis using the 85 K scan corroborates the former.

The final result that emerges from these three independent analysis methods for the localization of phosphorus in phosphated ZSM-5 is that of three approximate positions (P1, P2, and P3 in Table 3) at which the phosphate groups tend to be located. Apparently, there is sufficient randomness to prevent a more detailed localization of the individual atoms.

3.2. Short-Range Order: Total Scattering Analysis.

Having solved the position of the phosphate groups with XRD and ND in the previous paragraphs, we are now looking into the short-range order, which we derive from total scattering analysis. This technique uses information present in the X-ray and neutron diffraction patterns in a different way.[55]

Pair distribution functions were calculated from synchrotron XRD data specifically collected for this purpose and from ND data measured at 1.098 Å, allowing for data at higher *Q*-values to be included. The structure solutions obtained from synchrotron XRD were used to fit the patterns, but not refined. A reasonable fit was observed (see Figure 3), although

https://dx.doi.org/10.1021/acs.chemmater.0c03411
Chem. Mater. 2020, 32, 9390−9403

some small deviations can be observed at r = 4 Å and higher. It proved impossible to perform a full profile fit by refining the atom positions, as there are too many variables to provide a meaningful fit of the limited data set. In addition, the software we used for fitting the patterns does not allow for restraints on these parameters. The patterns for the phosphated material (0.8 P/Al, Figure 3c,d) showed a much poorer fit, especially in the low-r region, indicating that the short-range local order is not well described by the X-ray structure solutions, in keeping with the large Debye−Waller factors found in refinement, as well as with the fact that the positions of the individual O atoms could not be located.

In studying the high resolution X-ray PDFs for the two phosphated samples compared to the parent material (see Figure 4), a small shift in the first peak (T−O bond) position was observed. This can be completely explained by a contribution from a bond at about 1.54 Å, which is the bond length for the P−O bond that increases with the P content (Figure 4b).

3.3. Strain in the Framework: Temperature-Dependent Monoclinic−Orthorhombic Transition. The MFI structure is known to shift between a low-temperature monoclinic form and a high-temperature orthorhombic form.[56−60] The transition temperature between these crystal classes, visible in temperature-programed XRD, depends on the framework composition and lattice strain (e.g., the presence of phosphorus in the pores). We expect phosphorus in the pores and possibly the framework dealumination to have an effect on the transition temperature.

In Figure 5 we show the effect of temperature on the phase transition in a series of temperature-programed synchrotron powder XRD experiments. The monoclinic structure presents itself by the splitting of the 133 peak (a single peak in the orthorhombic structure) into the −313/313 doublet in the Q = 1.72−1.74 $Å^{-1}$-range. High-SAR ZSM-5 is known to be monoclinic at room temperature and orthorhombic at temperatures higher than about 100−125 °C. This is illustrated in Figure 5a for a high SAR ZSM-5 (Si/Al: 120, no P treatment).

Lower SAR materials may show a lower transition temperature, causing these to display orthorhombic symmetry at room temperature. Figure 5b−f shows the parent material, 0.8 P/Al HZSM-5 and 5.0 P/Al HZSM-5 samples, the steamed parent material, and a Si/Al 41.5 sample for comparison.

Unexpectedly, both the parent material and the 0.8 P/Al HZSM-5 sample show no signs of the monoclinic structure (see Figure 5b,c) at 85 K. The introduction of P in this sample does not influence the temperature behavior of the phase transition. The 5.0 P/Al sample (Figure 5d) clearly shows the monoclinic split[61] and is converted to an orthorhombic structure around room temperature (which is why it was labeled as orthorhombic in the previous paper from our group, based on lab-XRD data[32]). The transitions for the steamed parent material and the SAR 41.5 sample roughly follow the same path as 5.0 P/Al ZSM-5. The transition trajectory for these samples is spread over a much larger temperature range (200 °C) than for the high-SAR material (50 °C). We attribute the monoclinicity of the steamed parent and 5.0 P/Al ZSM-5 samples to extensive framework dealumination, which converts at least part of the material to (highly damaged) high-SAR ZSM-5. The framework damage (and possibly the presence of extra framework Al in the pores) is then responsible for the larger transition trajectory. The effect of this framework damage is similar to increasing the framework SAR (Figure 5e) or severe steaming (Figure 5f). In the samples we examined, we thus do not observe any effect of the presence of P in the structure on the monoclinic−orthorhombic transition. However, the absence of transition in the 0.8 P/Al sample must imply that there is no major framework damage for this sample, in spite of the obvious reaction of the framework with phosphate found with XRD.

4. COMPUTATIONAL STUDY

In the Results and Discussion section, we derived a model in which phosphate groups are found in crystallographically defined positions in the pores. In this section, we will use molecular modeling to investigate the likelihood of formation of some of our suggested structures for the interaction of P with Al. We perform our calculations on a fixed periodic unit cell with no imposed symmetry, in which one of the T atoms in the T12 position is an Al atom and all other T atoms are Si. To a certain extent, our results can be compared to the cluster calculations of Huang et al.,[62] who studied adsorption of phosphate species and reaction with the framework on small clusters around T6, T9, and T12 atoms. Lü et al.[63,64] compared cluster models derived from the models proposed by Kaeding and Lercher and concluded that Lercher's model is the more favorable of the two. Small-cluster calculations, of course, underestimate the effects of confinement and strain in the framework, so a direct comparison with our results is not particularly relevant. Huang et al.[62] reported binding energies of 21−25 kcal/mol for the binding of phosphate to the different T sites and found the product of reacting phosphate with the cluster to be similar to the one proposed by Kaeding and Butter[19] Abubakar et al.[10] reported an adsorption energy of 27.9 kcal/mol for H_3PO_4 on the bridging Si−OH−Al bond, which was also based on cluster calculations. None of these papers investigated the combined result of the actions of water and phosphate on the ZSM-5 structure. We will compare the relative energies of essentially all literature models in periodic calculations for the first time and will allow for the combination of hydrolysis by steam and phosphatation.

The starting structure for the modeling study was derived from an optimization of the MFI framework starting from two different structures: the single-crystal structure reported by Olson et al.[54] and a DLS-76[65] optimization of the coordinates taken from the website of the International Zeolite Association.[66] The DLS76-derived structure leads to a solution with an energy that is 13.3 kcal/mol more favorable than the Olson structure (both structures retain the same framework topology) and appears to be more regular upon visual inspection. We used the optimized DLS structure as the starting point for our further study.

We calculated the reaction energies between the MFI framework and reactants, water and phosphoric acid, to model steaming and phosphatation of the framework. We only calculated the electronic reaction energies (i.e., no accounting for zero-point energy or thermal contributions) and we did not search for transition states. We typically report energies compared to the free, unreacted components, that is, the MFI framework with one aluminum atom replacing one of the T12 positions, and a charge compensating proton on one of the four oxygens, free water, and free phosphoric acid, all calculated in the same unit cell volume.

There is a large body of work combining theoretical and experimental evidence for the possible locations of Al atoms in

https://dx.doi.org/10.1021/acs.chemmater.0c03411
Chem. Mater. 2020, 32, 9390−9403

the different T sites, going back to the work of Derouane and Fripiat et al. in 1983 and 1985.[67,68] These authors used quantum-chemical studies to study the locations in small (monomeric and pentameric) clusters and found T2 and T12 to be favored. A later computational work by Lonsinger et al.[69] found T12 to be the most preferred site in studies on 8-T atom clusters. Since then, many others have studied the problem, several concluding on T12 as the preferred site.[70−73] In a recent perspective describing both theoretical and experimental works, Knott et al.[74] summarized this, concluding that the T12 site is the most frequently chosen. As T12 is on the intersection between the straight and sinusoidal channels and it is accessible for water attack anti to the Si−OH−Al bond, we selected T12 as our Al site.

The energies we calculate are not absolute electronic energies. We use a pseudopotential method; therefore, the energies are calculated relative to a fixed but arbitrary reference point. This implies that the differences are physically meaningful as the reference energies cancel out. Our reference points are defined as follows: "MFI" is the energy calculated for the MFI framework with one T12 silicon replaced by aluminum, "H_2O" is the energy calculated for a molecule of water in an otherwise empty unit cell (fixed at a = 20.12343 Å, b = 19.95413 Å, c = 13.42174 Å, and $\alpha = \beta = \gamma = 90°$), and "$H_3PO_4$" is the energy calculated for a molecule of H_3PO_4 in an otherwise empty unit cell. Table 4 provides the energies

Table 4. Energies of Selected Reference Structures.

structure	description	Hartree a.u.	kcal/mol
MFI	protonated ZSM-5 with Al on T12	−3470.50163	−217,7739.8
H_2O	water in vacuum	−17.22100	−10,806.2
H_3PO_4	H_3PO_4 in vacuum	−72.58916	−45,549.7
SILNEST	silanol nest, see below	−3470.07505	−2,177,472.1
$Al(OH)_3 \cdot 2H_2O$	hydrated EFAL, see below	−69.30950	−43,491.7

calculated in Hartree atomic units (a.u.) and kcal/mol. It should be noted that under typical calcination conditions of 1 atm partial water pressure and 823.15 K, the contribution of entropy to the gas phase Gibbs-free energy equals −44.2 kcal/mol. As most of the entropy is lost upon sorption of water on an Al atom and not recovered in subsequent reaction steps in the dealumination, the free energy differences are more positive than the electronic energies reported here. Dealumination is, in fact, a "rare event" on the nanosecond time scale.

In this work, we calculate only the energetics of the structures of interest. We have not calculated the transition states. When comparing the energies of our intermediate structures with recent works of Silaghi et al.[53] and Stanciakova et al.,[52] who studied dealumination pathways using different T atoms (T3, T10, and T11), we find our energies follow a very similar trend. Silaghi et al. reported that the dealumination reactions, in general, in the four structures they study (MOR, CHA, FAU, and MFI) show Brønsted−Evans−Polanyi behavior, that is, there is a more or less linear relation between the reaction energy and the activation energy. These observations make it unnecessary to calculate the transition states, as representative values are already given in the literature. Of course, to study the reaction pathways and conclude on the viability of specific routes and structures at increased temperatures and water vapor pressures, it would be better to calculate the Gibbs-free energies at elevated temperatures. Silaghi et al. and Stanciakova et al. provide insights into the procedures to do such calculations. A recent paper by Nielsen et al.[75] describes DFT-MD calculations on dealumination of H-SSZ-13 to find the reaction pathways at higher temperatures and the collective action of multiple water molecules. However, we use our calculations to compare with structures proposed in the literature by Huang et al.,[62] Lü et al.,[64] and Abubakar et al.,[10] and to illustrate the point that a combination of prior dealumination by hydrolysis with phosphate attack on dislodged species as a second step yields more viable structure models than those proposed in the literature, which only consider reactions of phosphate directly with lattice atoms or the Brønsted Si−OH−Al group.

The starting point for the calculations is the structure with one silicon atom in the ZSM-5-framework replaced by Al plus a charge-compensating proton. A cutout from this structure is shown in Figure 6a. We only show the atoms within a radius of

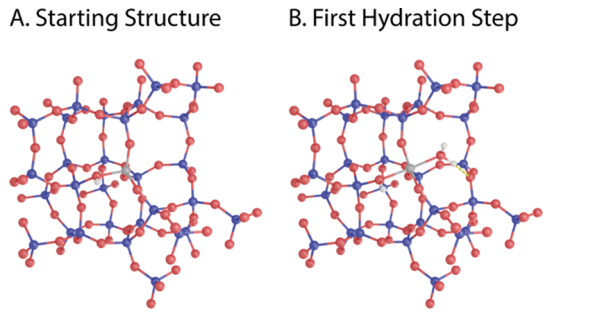

Figure 6. (a) Starting structure of all calculations. One of the silicon atoms in the T12 position of the ZSM-5 framework is replaced with an aluminum atom and one of the Si−O−Al bonds is protonated. Although we only show all atoms within a 7.5 Å radius of the Al atom, we calculated the full periodic structure. (b) Structure resulting after the first hydration step. The water molecule is positioned opposite to the Si−OH−Al bond.

7.5 Å from the Al atom and omit the rest of the periodic structure for clarity. The first hydration step occurs in a position directly opposite to the Si−OH−Al bond[53] and yields an energy gain of 7.9 kcal/mol compared to the reference structures (MFI + H_2O) [Figures 6b and 7 (step 1a)]. Transfer of a proton of the water molecule to the nearest Si−O−Al is endothermic by 1.2 kcal/mol compared to (MFI + H_2O). As a result, the original Si−O(H)−Al donative bond dissociates to form a silanol group (the Al−O bond is lost), and the proton from the water forms a new Si−O(H)−Al unit.

At this point, one of the original bonds of the aluminum atom in the framework is completely dislodged. The steps can be repeated three times (see Figure 7 and Table 5) to completely dislodge the Al atom from the framework and form $(H_2O)Al(OH)_3$, called Extra Framework ALuminum or EFAL. The final reaction step is the most exothermic step of the full dealumination pathway at −19.3 kcal/mol and may be the driving force for the dealumination and formation of EFAL (see Table S12 and Figure S33 in the Supporting Information for details on the individual steps of the dealumination pathway). As stated before, we did not compute transition states. We assume that these are not prohibitively high in energy and the pathway can be completed on a reasonable time scale.

https://dx.doi.org/10.1021/acs.chemmater.0c03411
Chem. Mater. 2020, 32, 9390−9403

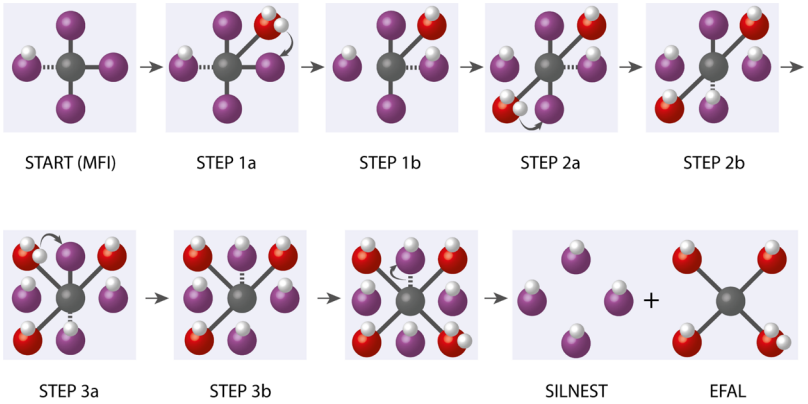

Figure 7. Schematic illustration of the dealumination steps through hydrolysis with steam. Detailed structures resulting from the calculations similar to Figure 6 can be found in the Supporting Information. Red spheres: oxygen; purple: oxygen connected to a framework silicon; gray: aluminum; and white: hydrogen.

Table 5. Relative Energies of Hydrolysis Steps[a]

	dealumination step	reference point	relative energy (kcal/mol)
1b	hydrolysis of the first bond	MFI + H_2O	+1.2
2b	hydrolysis of the second bond	MFI + $2H_2O$	+2.1
3b	hydrolysis of the third bond	MFI + $3H_2O$	+3.9
EFAL[b]	hydrolysis of the final bond, $(H_2O)Al(OH)_3$ in the pore	MFI + $4H_2O$	−19.3

[a]Only the final energies are reported; the intermediate steps are reported in the Supporting Information, Table S12. [b]EFAL: Extra Framework ALuminum.

The next step is to calculate the possible reactions of phosphate with the zeolite framework and the partially dislodged Al species. We start by calculating the relative energies for the literature models described above for comparison. Table 6 reports the energies found. The model of Lercher[27] is indeed more favorable than the model of Kaeding,[19] in agreement with the cluster results of Lü et al.,[63,64] but it is clear that this is not the most favorable model. Most of the models proposed in the literature do not provide energetically favored structures, apart from the hydrogen-bridged model proposed by Abubakar et al.[10]

Both Blasco et al.[5] and Abubakar et al.[10] proposed structures resulting from the reaction of the P═O (P−O double bond) group of phosphate with the Brønsted OH group in the Si−OH−Al bond. The proton transfer proposed by Blasco is not observed in our calculations, and the structure proposed by Abubakar is the final structure. Our value for the adsorption energy is in good agreement with the value of −27.9 kcal/mol reported by Abubaker et al. based on cluster calculations.[10] In the Supporting Information, we provide the results of an additional number of direct reactions between phosphate and the MFI framework. These reactions, which involve options for the formation of Si−O−P bonds (like the Lercher model), also prove to be not energetically favorable. While we observe the formation of Si−O−P bonds in our previous study,[32] this is most likely accompanied by lattice damage. Si−O−P bond formation in the intact framework is therefore unlikely, but these bonds can be formed in amorphous silicates resulting from (local) lattice collapse.

It thus appears that the model by Abubakar et al. is the most favorable literature model. The structure reported by Abubakar et al.[10] proves stable against hydration, as demonstrated in the Supporting Information. We will now move on to the reaction of phosphate with the partially dealuminated ZSM-5 framework, starting off with the structure with one dislodged framework bond (Figure 7, Step 1b). The condensation of one of the P−OH groups of phosphate with the dangling hydroxyl on the Al atom yields a structure similar to the one proposed by Zhuang et al.[7] Details on the approach and intermediate steps can be found in the Supporting Information, Section 5.3. The reaction [Figure 8 (top)] is exothermic by −4.2 kcal/mol compared to that of (MFI + H_3PO_4).

This structure can also be obtained by the direct reaction of a P−OH group of H_3PO_4 with the original Al12 site and moving the proton to an Si−O−Al moiety (which is the reaction proposed by Zhuang et al.[7]). The energies should be the same, and we indeed find an energy of −4.0 kcal/mol for

Table 6. Relative Energies for Structures Proposed in the Literature

model	illustration	reference point	relative energy (kcal/mol)
Kaeding[19]	Figure 1a	MFI + H_3PO_4 − H_2O	+10.4
Zhuang[7]	Figure 1b	MFI + H_3PO_4	−4.0[a]
Xue[13]	Figure 1c	MFI2AL + H_3PO_4 − $2H_2O$[b]	+35.2
van der Bij[22]	Figure 1d	MFI + $2H_3PO_4$ − H_2O	+3.8[a]
Blasco[5]/Abubakar[10]	Figure 1e,h	MFI + H_3PO_4	−29.0 (Abubakar model)
Lercher[27]	Figure 1f	MFI + H_3PO_4 − H_2O	+5.3
Caro[6]	Figure 1g	MFI + $4H_3PO_4$	+4.8

[a]The structure proposed by Zhuang also follows from the phosphatation of single-dislodged Al in this work. The structure proposed by van der Bij is calculated as step PIIc-2 in Table 7. [b]The structure proposed by Xue et al. requires a different reference point for the framework, which contains 2 Al atoms. The structure cannot be constructed as depicted in Figures 1 and 10, see the Supporting Information for further details.

https://dx.doi.org/10.1021/acs.chemmater.0c03411
Chem. Mater. 2020, 32, 9390−9403

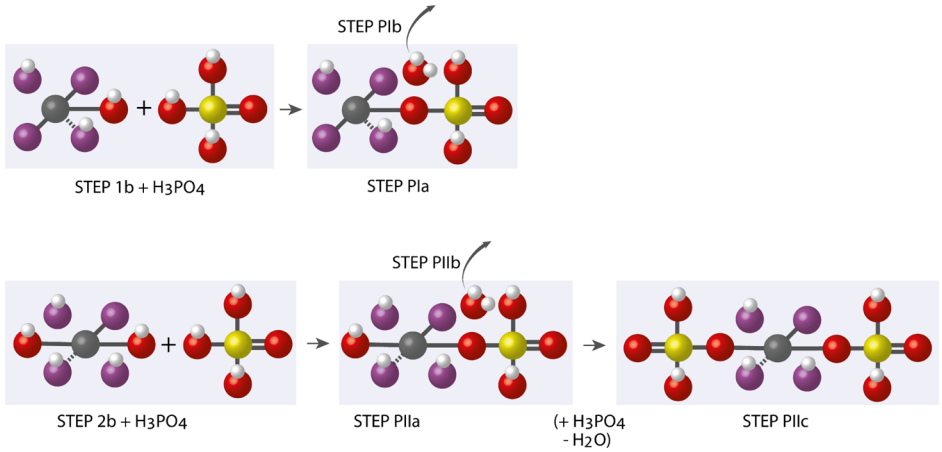

Figure 8. Reactions of phosphoric acid with partially dislodged framework Al atoms. Red spheres: oxygen; purple: oxygen connected to a framework silicon; gray: aluminum; white: hydrogen; and yellow: phosphorus.

this structure. The small difference is caused by the slightly different hydrogen bonds. Energies for the structures resulting from subsequent steps are listed in Table 7. It appears as though the structure in which the Al is bound to the framework by two remaining bonds is especially stable after reaction with one or more phosphate groups.

Table 7. Relative Energies of Phosphatation Steps[a]

	phosphatation step	reference point	relative energy (kcal/mol)
PIb	phosphatation of the result of step 1b	MFI + H_3PO_4	−4.2
PIIb	phosphatation of the result of step 2b	MFI + H_2O + H_3PO_4	−25.2
PIIc	second phosphatation of PIIb **on Al**	MFI + $2H_3PO_4$	−29.7
PIIc-2	condensation of P−OH groups in PIIc	MFI + $2H_3PO_4$ − H_2O	+3.8
PIId	second phosphatation of PIIb **on P**	MFI + $2H_3PO_4$	−23.1
PIIIb	phosphatation of the result of step 3b	MFI + $2H_2O$ + H_3PO_4	−0.9
PIV	phosphatation of EFAL	MFI + $3H_2O$ + H_3PO_4	−26.5

[a]Only the final energies are reported, the intermediate steps are reported in the Supporting Information.

The phosphated doubly dislodged Al species can react energetically favorably with a second phosphate group both by condensation of the second Al−OH (Table 7, PIIc) or by the formation of a two-membered polyphosphate chain (Table 7, PIId). This may explain why polyphosphate chains are observed in ^{31}P MAS-NMR in our previous paper.[32] While the reaction of doubly dislodged Al with 2 H_3PO_4 moieties is clearly highly favored, the final condensation of two phosphate groups (Table 7, PIIc-2) to form the structure, as proposed by van der Bij et al.,[22] seems energetically not favored.

The OH groups of phosphate are expected to be acidic. We therefore examined the adsorption of ammonia at the site IIb (Table 7). The adsorption of ammonia onto the Brønsted acid proton on the starting structure MFI is exothermic by −31.9 kcal/mol. Adsorption of ammonia onto one of the P−OH groups in structure IIb is exothermic by −31.8 kcal/mol, that is, the P−OH protons (as observed in the NMR spectra in our previous study[32]) exhibit the same acid strength as those of the original Brønsted sites. At the same time, the phosphate groups in the pores clearly block the pores and reduce the accessibility of the acid sites. The observed acidity is thus a compromise between these mechanisms. The Al atom in this structure can also act as a Lewis acid: ammonia adsorption is exothermic by −14.5 kcal/mol.

It should be noted that the results of the calculations are very dependent on the formation of hydrogen bonds. In many cases, there are several possibilities for forming hydrogen bond networks, all representing local minima. The expected deviations in the reported energies are on the order of one to at most a few kcal/mol, so this will not affect the general conclusions. At the increased temperature of the FCC process, the real system will achieve a dynamic equilibrium between all possible hydrogen bonding networks.

Our computed reaction energies strongly suggest that the reaction of phosphate with the doubly dislodged $Al(OH)_2$ moiety (see Figure 9a) and the reaction of phosphate with

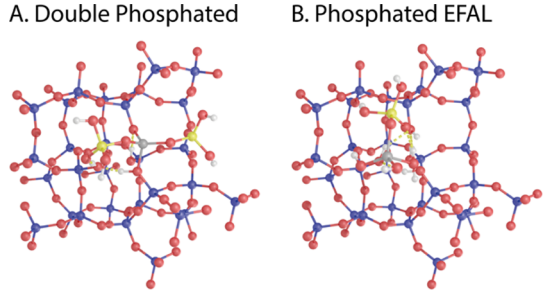

Figure 9. Energetically most favored phosphatation products. (a) The result of reacting two H_3PO_4 molecules with the doubly hydrolyzed structure. This reaction has an energy of −29.7 kcal/mol compared to that of (MFI + $2H_3PO_4$). (b) Product of the reaction of (hydrated) EFAL with H_3PO_4. This structure's energy is −26.5 kcal/mol compared to (MFI + $3H_2O$ + H_3PO_4).

EFAL (see Figure 9b) are the energetically most favorable routes combining dealumination and phosphatation effects. Both lead to phosphated Al species in the pores. We have thus provided new models that are as favorable energetically as the most successful model in the literature. It should be noted that all three models that are energetically favored are stable toward hydrolysis by water (the two models proposed here are

https://dx.doi.org/10.1021/acs.chemmater.0c03411
Chem. Mater. 2020, 32, 9390−9403

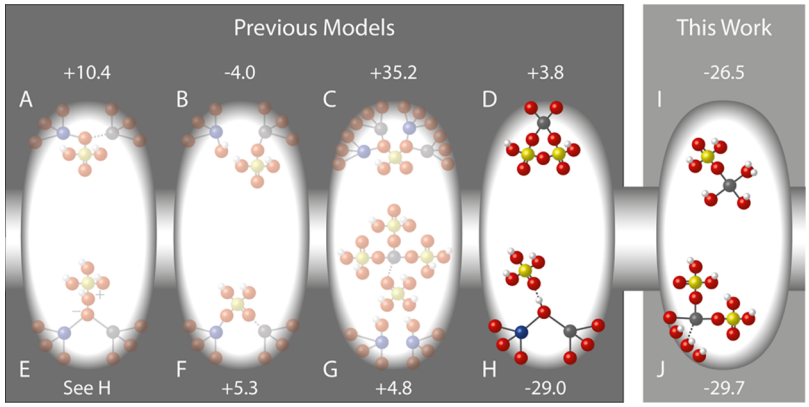

Figure 10. Overview of the proposed models in the literature, with their calculated relative energy in kcal/mol. (a) Kaeding and Butter,[19] (b) Zhuang et al.,[7] (c) Xue et al.,[13] (d) van der Bij et al.,[22] (e) Blasco et al.,[5] (f) Lercher et al.,[27] (g) Caro et al.,[6] and (h) Abubakar et al.;[10] This work: Two models are found that are energetically most favored. (i) A phosphated EFAL species is portrayed. This model, although energetically favored, will not be observed in XRD patterns because of its high rotational and translational degrees of freedom. (j) The bottom model portrays the structure of the other energetically favored model. Phosphate species are found in the pore system of the zeolite and are immobilized sufficiently to be observed in XRD and ND. They are tethered to partially dislodged framework Al species that have lost one or more direct bonds to the framework. In this model, two bonds have been lost and two remain. The P−OH groups in this model are acidic and (more than) compensate for the loss of the original Brønsted sites, explaining the stabilization/activation. The presence of tethered phosphate groups inside the pores explains the loss of surface area and accessibility of P-activated ZSM-5.

explicitly formed by condensation; for the model proposed by Abubakar, we specifically examined the stability, as described in the Supporting Information). We have only examined Al in one of the possible 12 T sites in our calculations but expect similar species to be formed on the other possible locations. The structure solutions found with the X-ray and neutron diffraction studies provide an average of all these possible solutions. We expect the phosphated EFAL species to be mobile to the extent that it would probably diffuse out of the pore system. The additional degrees of freedom and mobility compared to the tethered models would make it very unlikely that we would observe the phosphated EFAL in the diffraction analyses.

5. CONCLUSIONS

In this work, we examined a phosphate-activated ZSM-5 sample (0.8 P/Al ratio) alongside its untreated parent material to determine the location of the phosphorus within the pores of the material, hereby attempting to understand its activating or promotional effect in propylene-selective FCC catalysis. We locate phosphate species in phosphorus-stabilized ZSM-5 in partially occupied crystallographically defined positions with synchrotron powder XRD analysis at RT and 85 K. Two independent analytical approaches (difference Fourier analysis and rigid body PO_4 tetrahedron addition) yield similar structure solutions. Phosphate groups can be located in both the straight and zigzag channels of the ZSM-5. The room-temperature structure was further refined using a combination of XRD and ND analyses in a single refinement. Total scattering analysis on the XRD and ND patterns showed a larger local disorder than that observed in the XRD solutions for the phosphated sample. The presence of phosphate groups could be demonstrated by a small contribution at a bond length typical for P−O bonds. Phosphate introduction did not lead to observable changes in the monoclinic−orthorhombic transition, whereas framework damage through steaming or acid attack did induce changes in the monoclinic−orthorhombic transition. The P treatment of the ZSM-5 sample with Al at a ratio of 0.8, therefore, did not introduce massive framework damage.

We have made a comprehensive comparison of all literature models for the interaction of phosphate with the ZSM framework using periodic models for the first time. We conclude that, of these models, only the structure proposed by Abubakar et al.[10] is energetically favored; however, it does not take into account dealumination by steaming prior to phosphatation. Molecular modeling which takes into account the combination of dealumination and phosphatation shows that a structure where the aluminum atoms in the framework are partially dislodged and stabilized by phosphate groups is energetically favorable to a slightly higher extent than the model proposed by Abubakar et al.[10] Locating the phosphate groups in the pores of ZSM-5 corroborates previous APT results from our group, and the modeling work suggests that the new P−OH acid sites introduced by the phosphate stabilization can yield Brønsted acid sites of similar strength compared to the normal Si−OH−Al sites (see overview Figure 10). It is important to note that the positions observed in the diffraction studies have only partial occupation. Full occupation would block the pore system of the zeolite material completely and render it essentially useless. The partial pore blockages can likely be circumvented by "detours" through the 3D-channel system for small molecules such as propylene. This may yield a partially blocked pore system not unlike the diffusion hurdles faced by small olefins in CHA zeolites in methanol-to-olefin reactions.

We therefore present a complete explanation for the stabilization and activation of ZSM-5 by phosphate. Aluminum atoms are found close to, or even tethered to, their original framework positions, and react with phosphate to form stable immobile Si−O−Al−O−P structures. These Si−O−Al−O−P structures are acidic by themselves because of the protons in the phosphate groups. These protons are just as acidic as the normal Brønsted acid proton, as measured by their ammonia adsorption energies.

https://dx.doi.org/10.1021/acs.chemmater.0c03411
Chem. Mater. 2020, 32, 9390−9403

■ ASSOCIATED CONTENT

Supporting Information

The Supporting Information is available free of charge at https://pubs.acs.org/doi/10.1021/acs.chemmater.0c03411.

Methods and materials; structure refinement solutions; XRD analysis results; TOPAS input files; CP2K input files; and detailed information on theoretical modeling (PDF)

Original data for the XRD, X-ray-PDF, and ND experiments (ZIP)

■ AUTHOR INFORMATION

Corresponding Author

Eelco T.C. Vogt − *Albemarle Catalysts Company BV, 1022 AB Amsterdam, The Netherlands; Inorganic Chemistry and Catalysis Group, Debye Institute for Nanomaterials Science, Utrecht University, 3584 CG Utrecht, the Netherlands;* orcid.org/0000-0003-4556-4283; Email: E.T.C.Vogt@uu.nl

Authors

Jaap N. Louwen − *Albemarle Catalysts Company BV, 1022 AB Amsterdam, The Netherlands*

Lambert van Eijck − *Department NPM2/RST, Faculty of Applied Sciences, Delft University of Technology, 2629 JB Delft, The Netherlands*

Charlotte Vogt − *Department of Chemical and Biological Physics, Weizmann Institute of Science, 7610001 Rehovot, Israel; Institute of Chemistry and The Center for Nanoscience and Nanotechnology, Hebrew University of Jerusalem, 9190401 Jerusalem, Israel*

Complete contact information is available at: https://pubs.acs.org/10.1021/acs.chemmater.0c03411

Notes

The authors declare no competing financial interest.

■ ACKNOWLEDGMENTS

This research is part of the Strategic Theme Sustainability of Utrecht University and a related subsidy. This work was further supported by the Netherlands Organization for Scientific Research (NWO) (grant number TKINCI-2015.005). The authors would like to acknowledge Mauro Coduri, Ad van der Eerden, and Dr. Rosa Danisi for scientific and experimental support during the collection of the high-resolution XRPD data (ESRF experiment No CH-4998); the authors thank Dr. Hasnaa Mouttaki at Albemarle and Dr. Martin Lutz at the University of Utrecht for valuable discussions. C.V. acknowledges support by a Niels Stensen Fellowship. J.N.L. and E.T.C.V. acknowledge support by Albemarle Catalysts Company BV.

■ REFERENCES

(1) Vogt, E. T. C.; Weckhuysen, B. M. Fluid Catalytic Cracking: Recent Developments on the Grand Old Lady of Zeolite Catalysis. *Chem. Soc. Rev.* **2015**, *44*, 7342−7370.

(2) Hamada, R.; Watabe, M. More Propylene in FCC Units. *Proceedings of the 18th Annual Saudi-Japan Symposium on Catalysts in Petroleum Refining and Petrochemicals*, 2008, https://catsymp.kfupm.edu.sa/docs/18%20Symppsium%20Papers/07%20JGC.pdf accessed Oct 5, 2020.

(3) Akah, A.; Al-Ghrami, M. Maximizing Propylene Production via FCC Technology. *Appl. Petrochem. Res.* **2015**, *5*, 377−392.

(4) Knight, J.; Mehlberg, R. Maximize Propylene. *Hydrocarbon Process.* **2011**, *90*, 91−95.

(5) Blasco, T.; Corma, A.; Martinez-Triguero, J. Hydrothermal Stabilization of ZSM-5 Catalytic-Cracking Additives by Phosphorus Addition. *J. Catal.* **2006**, *237*, 267−277.

(6) Caro, J.; Bülow, M.; Derewinski, M.; Haber, J.; Hunger, M.; Kärger, J.; Pfeifer, H.; Storek, W.; Zibrowius, B. NMR and IR Studies of Zeolite H-ZSM-5 Modified with Orthophosphoric Acid. *J. Catal.* **1990**, *124*, 367−375.

(7) Zhuang, J.; Ma, D.; Yang, G.; Yan, Z.; Liu, X.; Liu, X.; Han, X.; Bao, X.; Xie, P.; Liu, Z. Solid-State MAS NMR Studies on the Hydrothermal Stability of the Zeolite Catalysts for Residual Oil Selective Catalytic Cracking. *J. Catal.* **2004**, *228*, 234−242.

(8) Zhao, G.; Teng, J.; Xie, Z.; Jin, W.; Yang, W.; Chen, Q.; Tang, Y. Effect of Phosphorus on HZSM-5 Catalyst for C4-Olefin Cracking Reactions to Produce Propylene. *J. Catal.* **2007**, *248*, 29−37.

(9) Liu, J.; Zhang, C.; Shen, Z.; Hua, W.; Tang, Y.; Shen, W.; Yue, Y.; Xu, H. Methanol to Propylene: Effect of Phosphorus on a High Silica HZSM-5 Catalyst. *Catal. Commun.* **2009**, *10*, 1506−1509.

(10) Abubakar, S. M.; Marcus, D. M.; Lee, J. C.; Ehresmann, J. O.; Chen, C.-Y.; Kletnieks, P. W.; Guenther, D. R.; Hayman, M. J.; Pavlova, M.; Nicholas, J. B.; Haw, J. F. Structural and Mechanistic Investigation of a Phosphate-Modified HZSM-5 Catalyst for Methanol Conversion. *Langmuir* **2006**, *22*, 4846−4852.

(11) Cabral de Menezes, S. M.; Lam, Y. L.; Damodaran, K.; Pruski, M. Modification of H-ZSM-5 Zeolites with Phosphorus. 1. Identification of Aluminum Species by 27Al Solid-State NMR and Characterization of Their Catalytic Properties. *Microporous Mesoporous Mater.* **2006**, *95*, 286−295.

(12) Damodaran, K.; Wiench, J. W.; Cabral de Menezes, S. M.; Lam, Y. L.; Trebosc, J.; Amoureux, J.-P.; Pruski, M. Modification of H-ZSM-5 Zeolites with Phosphorus. 2. Interaction between Phosphorus and Aluminum Studied by Solid-State NMR Spectroscopy. *Microporous Mesoporous Mater.* **2006**, *95*, 296−305.

(13) Xue, N.; Chen, X.; Nie, L.; Guo, X.; Ding, W.; Chen, Y.; Gu, M.; Xie, Z. Understanding the Enhancement of Catalytic Performance for Olefin Cracking: Hydrothermally Stable Acids in P/HZSM-5. *J. Catal.* **2007**, *248*, 20−28.

(14) Song, Z.; Takahashi, A.; Nakamura, I.; Fujitani, T. Phosphorus-Modified ZSM-5 for Conversion of Ethanol to Propylene. *Appl. Catal., A* **2010**, *384*, 201−205.

(15) Göhlich, M.; Reschetilowski, W.; Paasch, S. Spectroscopic Study of Phosphorus Modified H-ZSM-5. *Microporous Mesoporous Mater.* **2011**, *142*, 178−183.

(16) Janardhan, H. L.; Shanbhag, G. V.; Halgeri, A. B. Shape-Selective Catalysis by Phosphate Modified ZSM-5: Generation of New Acid Sites with Pore Narrowing. *Appl. Catal., A* **2014**, *471*, 12−18.

(17) Yamaguchi, A.; Jin, D.; Ikeda, T.; Sato, K.; Hiyoshi, N.; Hanaoka, T.; Mizukami, F.; Shirai, M. P-ZSM-5 Pretreated by High-Temperature Calcination as Durable Catalysts for Steam Cracking of n-Hexane. *Catal. Lett.* **2013**, *144*, 44−49.

(18) van der Bij, H. E.; Aramburo, L. R.; Arstad, B.; Dynes, J. J.; Wang, J.; Weckhuysen, B. M. Phosphatation of Zeolite H-ZSM-5: A Combined Microscopy and Spectroscopy Study. *ChemPhysChem* **2014**, *15*, 283−292.

(19) Kaeding, W.; Butter, S. Production of chemicals from methanol I. Low molecular weight olefins. *J. Catal.* **1980**, *61*, 155−164.

(20) Vinek, H.; Rumplmayr, G.; Lercher, J. A. Catalytic Properties of Postsynthesis Phosphorus-Modified H-ZSM5 Zeolites. *J. Catal.* **1989**, *115*, 291−300.

(21) Kojima, M.; Lefebvre, F.; Ben Taârit, Y. Modification of Siliceous Zeolites Using Phosphorus Pentachloride. *Zeolites* **1992**, *12*, 724−727.

(22) van der Bij, H. E.; Weckhuysen, B. M. Local Silico-Aluminophosphate Interfaces within Phosphated H-ZSM-5 Zeolites. *Phys. Chem. Chem. Phys.* **2014**, *16*, 9892−9903.

(23) Losch, P.; Laugel, G.; Martinez-Espin, J. S.; Chavan, S.; Olsbye, U.; Louis, B. Phosphorous Modified ZSM-5 Zeolites: Impact on Methanol Conversion into Olefins. *Top. Catal.* **2015**, *58*, 826−832.
(24) van der Bij, H. E.; Meirer, F.; Kalirai, S.; Wang, J.; Weckhuysen, B. M. Hexane Cracking over Steamed Phosphated Zeolite H-ZSM-5: Promotional Effect on Catalyst Performance and Stability. *Chem.—Eur. J.* **2014**, *20*, 16922−16932.
(25) Caeiro, G.; Magnoux, P.; Lopes, J. M.; Ribeiro, F. R.; Menezes, S. M. C.; Costa, A. F.; Cerqueira, H. S. Stabilization Effect of Phosphorus on Steamed H-MFI Zeolites. *Appl. Catal., A* **2006**, *314*, 160−171.
(26) Lischke, G.; Eckelt, R.; Jerschkewitz, H.-G.; Parlitz, B.; Schreier, E.; Storek, W.; Zibrowius, B.; Öhlmann, G. Spectroscopic and Physicochemical Characterization of P-Modified H-ZSM-5. *J. Catal.* **1991**, *132*, 229−243.
(27) Lercher, J. A.; Rumplmayr, G. Controlled Decrease of Acid Strength by Orthophosporic Acid on ZSM5. *Appl. Catal.* **1986**, *25*, 215−222.
(28) Dyballa, M.; Klemm, E.; Weitkamp, J.; Hunger, M. Effect of Phosphate Modification on the Brønsted Acidity and Methanol-to-Olefin Conversion Activity of Zeolite ZSM-5. *Chem. Ing. Tech.* **2013**, *85*, 1719−1725.
(29) van der Bij, H. E.; Cicmil, D.; Wang, J.; Meirer, F.; de Groot, F. M. F.; Weckhuysen, B. M. Aluminum-Phosphate Binder Formation in Zeolites as Probed with X-Ray Absorption Microscopy. *J. Am. Chem. Soc.* **2014**, *136*, 17774−17787.
(30) Gao, X.; Tang, Z.; Zhang, H.; Liu, C.; Zhang, Z.; Lu, G.; Ji, D. High Performance Phosphorus-Modified ZSM-5 Zeolite for Butene Catalytic Cracking. *Korean J. Chem. Eng.* **2010**, *27*, 812−815.
(31) van der Bij, H. E.; Weckhuysen, B. M. Phosphorus Promotion and Poisoning in Zeolite-Based Materials: Synthesis, Characterisation and Catalysis. *Chem. Soc. Rev.* **2015**, *44*, 7406−7428.
(32) Danisi, R. M.; Schmidt, J. E.; Lucini Paioni, A.; Houben, K.; Poplawsky, J. D.; Baldus, M.; Weckhuysen, B. M.; Vogt, E. T. C. Revealing Long- and Short-Range Structural Modifications within Phosphorus-Treated HZSM-5 Zeolites by Atom Probe Tomography, Nuclear Magnetic Resonance and Powder X-Ray Diffraction. *Phys. Chem. Chem. Phys.* **2018**, *20*, 27766−27777.
(33) Luna Murillo, B. Aromatization of Oxygenates over Zeolite Catalysts. Ph.D. Thesis, Utrecht University, The Netherlands, 2020.
(34) Kieffer, J.; Karkoulis, D. PyFAI, a Versatile Library for Azimuthal Regrouping. *J. Phys.: Conf. Ser.* **2013**, *425*, 202012.
(35) Kieffer, J.; Wright, J. P. PyFAI: A Python Library for High Performance Azimuthal Integration on GPU. *Powder Diffr.* **2013**, *28*, S339−S350.
(36) Juhás, P.; Davis, T.; Farrow, C. L.; Billinge, S. J. L. PDFgetX3: A Rapid and Highly Automatable Program for Processing Powder Diffraction Data into Total Scattering Pair Distribution Functions. *J. Appl. Crystallogr.* **2013**, *46*, 560−566.
(37) Van Eijck, L.; Cussen, L. D.; Sykora, G. J.; Schooneveld, E. M.; Rhodes, N. J.; Van Well, A. A.; Pappas, C. Design and Performance of a Novel Neutron Powder Diffractometer: PEARL at TU Delft. *J. Appl. Crystallogr.* **2016**, *49*, 1398−1401.
(38) Juhás, P.; Louwen, J. N.; van Eijck, L.; Vogt, E. T. C.; Billinge, S. J. L. PDFgetN3: Atomic Pair Distribution Functions from Neutron Powder Diffraction Data Using Ad Hoc Corrections. *J. Appl. Crystallogr.* **2018**, *51*, 1492−1497.
(39) Coelho, A. A. TOPAS and TOPAS-Academic: An Optimization Program Integrating Computer Algebra and Crystallographic Objects Written in C++. *J. Appl. Crystallogr.* **2018**, *51*, 210−218.
(40) f0_WaasKirf.dat. http://ftp.esrf.fr/pub/scisoft/xop2.3/DabaxFiles/f0_WaasKirf.dat (accessed March 20, 2020).
(41) LIST~1.HTM. http://www.ccp14.ac.uk/ccp/web-mirrors/neutrons/n-scatter/n-lengths/LIST?1.HTM (accessed March 20, 2020).
(42) Hutter, J.; Iannuzzi, M.; Schiffmann, F.; VandeVondele, J. CP2K: Atomistic Simulations of Condensed Matter Systems. *Wiley Interdiscip. Rev.: Comput. Mol. Sci.* **2014**, *4*, 15−25.
(43) Borštnik, U.; Vandevondele, J.; Weber, V.; Hutter, J. Sparse Matrix Multiplication: The Distributed Block-Compressed Sparse Row Library. *Parallel Comput.* **2014**, *40*, 47−58.
(44) Vandevondele, J.; Krack, M.; Mohamed, F.; Parrinello, M.; Chassaing, T.; Hutter, J. Quickstep: Fast and Accurate Density Functional Calculations Using a Mixed Gaussian and Plane Waves Approach. *Comput. Phys. Commun.* **2005**, *167*, 103−128.
(45) VandeVondele, J.; Hutter, J. An Efficient Orbital Transformation Method for Electronic Structure Calculations. *J. Chem. Phys.* **2003**, *118*, 4365−4369.
(46) Lippert, G.; Hutter, J.; Parrinello, M. A Hybrid Gaussian and Plane Wave Density Functional Scheme. *Mol. Phys.* **1997**, *92*, 477−488.
(47) Perdew, J. P.; Burke, K.; Ernzerhof, M. Generalized Gradient Approximation Made Simple. *Phys. Rev. Lett.* **1996**, *77*, 3865−3868.
(48) VandeVondele, J.; Hutter, J. Gaussian Basis Sets for Accurate Calculations on Molecular Systems in Gas and Condensed Phases. *J. Chem. Phys.* **2007**, *127*, 114105.
(49) Goedecker, S.; Teter, M.; Hutter, J. Separable Dual-Space Gaussian Pseudopotentials. *Phys. Rev. B: Condens. Matter Mater. Phys.* **1996**, *54*, 1703−1710.
(50) Hartwigsen, C.; Goedecker, S.; Hutter, J. Relativistic Separable Dual-Space Gaussian Pseudopotentials from H to Rn. *Phys. Rev. B: Condens. Matter Mater. Phys.* **1998**, *58*, 3641−3662.
(51) Krack, M. Pseudopotentials for H to Kr Optimized for Gradient-Corrected Exchange-Correlation Functionals. *Theor. Chem. Acc.* **2005**, *114*, 145−152.
(52) Stanciakova, K.; Ensing, B.; Göltl, F.; Bulo, R. E.; Weckhuysen, B. M. Cooperative Role of Water Molecules during the Initial Stage of Water-Induced Zeolite Dealumination. *ACS Catal.* **2019**, *9*, 5119−5135.
(53) Silaghi, M.-C.; Chizallet, C.; Sauer, J.; Raybaud, P. Dealumination Mechanisms of Zeolites and Extra-Framework Aluminum Confinement. *J. Catal.* **2016**, *339*, 242−255.
(54) Olson, D. H.; Kokotailo, G. T.; Lawton, S. L.; Meier, W. M. Crystal Structure and Structure-Related Properties of ZSM-5. *J. Phys. Chem.* **1981**, *85*, 2238−2243.
(55) Egami, T.; Billinge, S. J. L. *Underneath the Bragg Peaks: Structural Analysis of Complex Materials*, 2nd ed.; Elsevier, Amsterdam, 2012.
(56) Ardit, M.; Martucci, A.; Cruciani, G. Monoclinic-Orthorhombic Phase Transition in ZSM-5 Zeolite: Spontaneous Strain Variation and Thermodynamic Properties. *J. Phys. Chem. C* **2015**, *119*, 7351−7359.
(57) Hay, D. G.; Jaeger, H.; West, G. W. Examination of the Monoclinic-Orthorhombic Transition in Silicallte Using XRD and Silicon NMR. *J. Phys. Chem.* **1985**, *89*, 1070−1072.
(58) Chezeau, J. M.; Delmotte, L.; Hasebe, T.; Chanh, N. B. Low Temperature Orthorhombic-Monoclinic Transition in as-Synthesized MFI Siliceous Zeolites. *Zeolites* **1991**, *11*, 729−731.
(59) van Koningsveld, H.; Jansen, J. C.; van Bekkum, H. The Orthorhombic/Monoclinic Transition in Single Crystals of Zeolite ZSM-5. *Zeolites* **1987**, *7*, 564−568.
(60) Hay, D. G.; Jaeger, H. Orthorhombic-Monoclinic Phase Changes in ZSM-5 ZeolitelSilicalite. *J. Chem. Soc., Chem. Commun.* **1984**, 1433.
(61) Wu, E. L.; Lawton, S. L.; Olson, D. H.; Rohrman, A. C.; Kokotailo, G. T. ZSM-5-Type Materials. Factors Affecting Crystal Symmetry. *J. Phys. Chem.* **1979**, *83*, 2777−2781.
(62) Huang, Y.; Dong, X.; Li, M.; Zhang, M.; Yu, Y. Density Functional Theory Study of the Structural and Electronic Properties of H3PO4/ZSM-5. *RSC Adv.* **2014**, *4*, 14573.
(63) Lü, R.; Cao, Z.; Liu, X. Catalytic Activity of Phosphorus and Steam Modified HZSM-5 and the Theoretical Selection of Phosphorus Grafting Model. *J. Nat. Gas Chem.* **2008**, *17*, 142−148.
(64) Lü, R.; Cao, Z.; Wang, S. Density Functional Study on Models of Interaction between Phosphorus Species and HZSM-5. *J. Mol. Struct.: THEOCHEM* **2008**, *865*, 1−7.

https://dx.doi.org/10.1021/acs.chemmater.0c03411
Chem. Mater. 2020, 32, 9390−9403

(65) Baerlocher, C.; Hepp, A.; Meier, W. M.. *DLS-76: A Program for the Simulation of Crystal Structures by Geometric Refinement*; Institute of crystallography and petrography - ETH, 1978.
(66) Structure Commission of the International Zeolite Association. Database of Zeolite Structures, https://europe.iza-structure.org/IZA-SC/cif/MFI.cif (accessed July 26, 2019).
(67) Fripiat, J. G.; Berger-André, F.; André, J.-M.; Derouanc, E. G. Non-Empirical Quantum Mechanical Calculations on Pentasil-Type Zeolites. *Zeolites* **1983**, *3*, 306−310.
(68) Derouane, E. G.; Fripiat, J. G. Non-Empirical Quantum Chemical Study of the Siting and Pairing of Aluminium in the MFI Framework. *Zeolites* **1985**, *5*, 165−172.
(69) Lonsinger, S. R.; Chakraborty, A. K.; Theodorou, D. N.; Bell, A. T. The Effects of Local Structural Relaxation on Aluminum Siting within H-ZSM-5. *Catal. Lett.* **1991**, *11*, 209−217.
(70) Mentzen, B. F.; Sacerdote-Peronnet, M. Prediction of Preferred Proton Locations in HMFI/Benzene Complexes by Molecular Mechanics Calculations. Comparison with Nmr, Structural and Calorimetric Results. *Mater. Res. Bull.* **1994**, *29*, 1341−1348.
(71) Tranca, D. C.; Zimmerman, P. M.; Gomes, J.; Lambrecht, D.; Keil, F. J.; Head-Gordon, M.; Bell, A. T. Hexane Cracking on ZSM-5 and Faujasite Zeolites: A QM/MM/QCT Study. *J. Phys. Chem. C* **2015**, *119*, 28836−28853.
(72) Kim, S.; Robichaud, D. J.; Beckham, G. T.; Paton, R. S.; Nimlos, M. R. Ethanol Dehydration in HZSM-5 Studied by Density Functional Theory: Evidence for a Concerted Process. *J. Phys. Chem. A* **2015**, *119*, 3604−3614.
(73) Joshi, K. L.; Psofogiannakis, G.; Van Duin, A. C. T.; Raman, S. Reactive Molecular Simulations of Protonation of Water Clusters and Depletion of Acidity in H-ZSM-5 Zeolite. *Phys. Chem. Chem. Phys.* **2014**, *16*, 18433−18441.
(74) Knott, B. C.; Nimlos, C. T.; Robichaud, D. J.; Nimlos, M. R.; Kim, S.; Gounder, R. Consideration of the Aluminum Distribution in Zeolites in Theoretical and Experimental Catalysis Research. *ACS Catal.* **2018**, *8*, 770−784.
(75) Nielsen, M.; Hafreager, A.; Brogaard, R. Y.; De Wispelaere, K.; Falsig, H.; Beato, P.; Van Speybroeck, V.; Svelle, S. Collective Action of Water Molecules in Zeolite Dealumination. *Catal. Sci. Technol.* **2019**, *9*, 3721−3725.

https://dx.doi.org/10.1021/acs.chemmater.0c03411
Chem. Mater. 2020, 32, 9390−9403